Electronic Supplementary Material (ESI) for Physical Chemistry Chemical Physics.

Supplementary Information

X-ray spectroscopy characterization of azobenzene-functionalized triazatriangulenium adlayers on Au(111) surfaces

Sandra Ulrich[a], Ulrich Jung[b], Thomas Strunskus[c], Christian Schütt[a], Andreas Bloedorn[b], Sonja Lemke [b], Eric Ludwig[b], Lutz Kipp[b], Franz Faupel[c], Olaf Magnussen[b] and Rainer Herges[a]*

1. Additional XP spectra
2. Additional NEXAFS spectra
3. DFT Calculations
4. Synthesis

1. Additional XP spectra

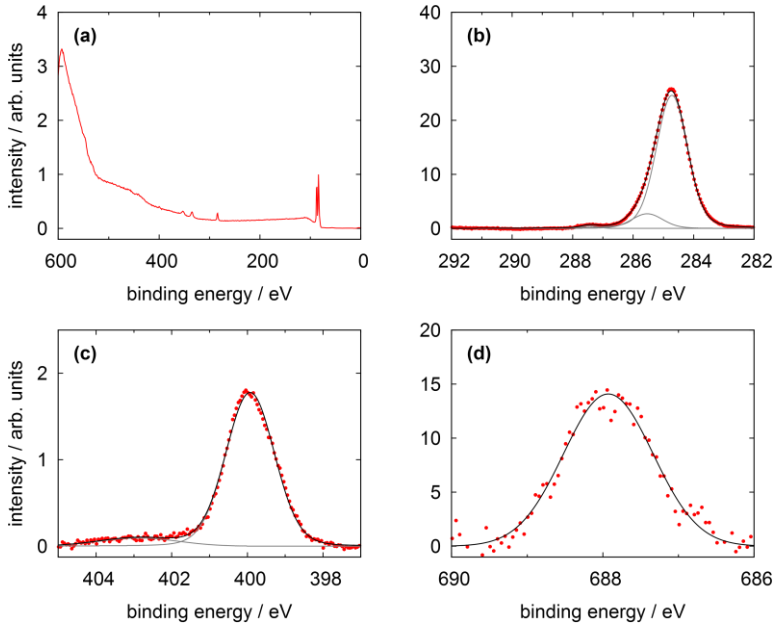

Figure S 1: XP spectra of a FAzo-TATA monolayer on Au(111) showing (a) a survey spectrum, (b) the C 1s, (c) the N 1s and (d) the F 1s region.

Table S 2: Quantitative analysis of the XPS results of FAzo-TATA monolayer. * Only the direct fitting errors are given. The total error cannot be inferred in a straight-forward manner and is estimated to be 15 %.

element	binding energy (eV)*	relative intensity*	calc. stoichiometry	assignment
C 1s	284.7 ± 0.1	0.885 ± 0.130	0.789	arom. + aliph.
	285.5 ± 0.1	0.098 ± 0.018	0.193	C-N
	287.4 ± 0.1	0.017 ± 0.003	0.018	C-F
N 1s	399.9 ± 0.1	0.064 ± 0.009	0.088	all N atoms
F 1s	687.9 ± 0.1	0.061 ± 0.027	0.018	all F atoms

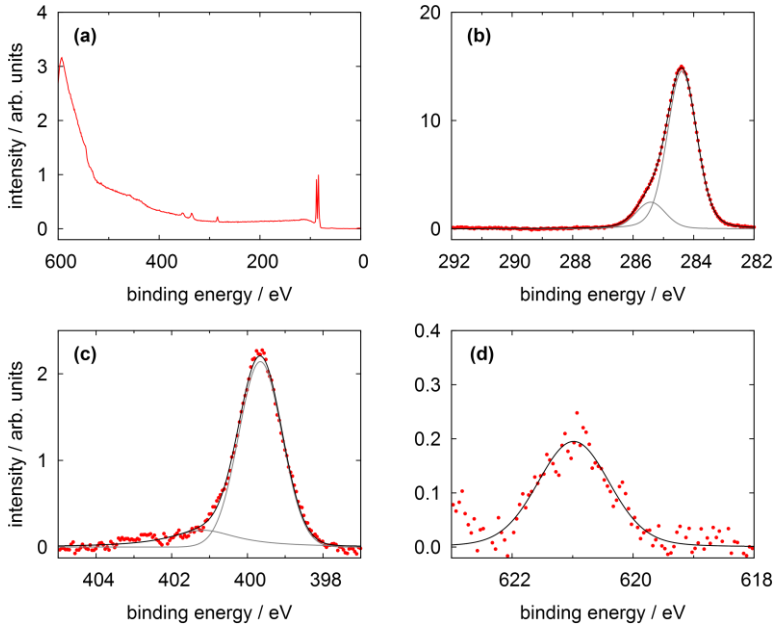

Figure S 3: XP spectra of a IAzo-TATA monolayer on Au(111) showing (a) a survey spectrum, (b) the C 1s, (c) the N 1s and (d) the I $3d_{5/2}$ region.

Table S 4: Quantitative analysis of the XPS results of IAzo-TATA monolayer. * Only the direct fitting errors are given. The total error cannot be inferred in a straight-forward manner and is estimated to be 15 %.

element	binding energy (eV)*	relative intensity*	calc. stoichiometry	assignment
C 1s	284.4 ± 0.1	0.856 ± 0.018	0.807	arom. + aliph.
	285.4 ± 0.1	0.144 ± 0.004	0.193	C-N
N 1s	399.7 ± 0.1	0.126 ± 0.003	0.088	all N atoms
I 3d	621.0 ± 0.1	0.004 ± 0.001	0.018	all I atoms

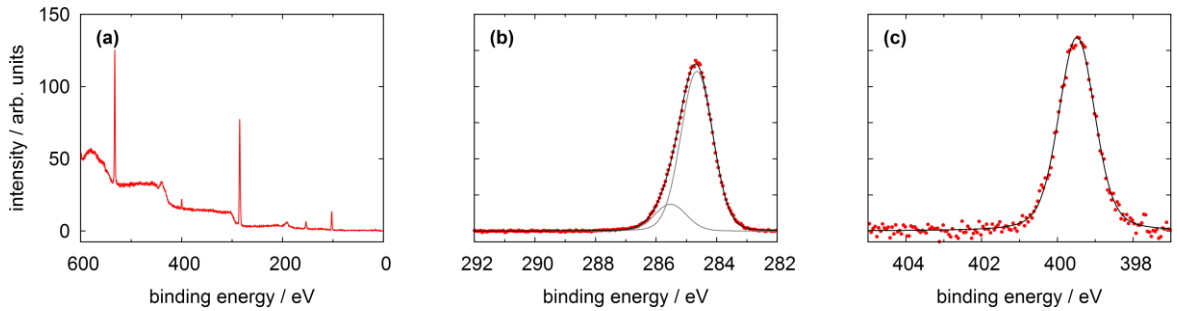

Figure S 5: XP spectra of a Me-TATA multilayer on Au(111) showing (a) a survey spectrum, (b) the C 1s and (c) the N 1s region.

Table S 6: Quantitative analysis of the XPS results of Me-TATA multilayer. * Only the direct fitting errors are given. The total error cannot be inferred in a straight-forward manner and is estimated to be 15 %.

element	binding energy (eV)*	relative intensity*	calc. stoichiometry	assignment
C 1s	284.7 ± 0.1	0.856 ± 0.071	0.795	arom. + aliph.
	285.5 ± 0.1	0.144 ± 0.016	0.205	C-N
N 1s	399.5 ± 0.1	-	0.068	all N atoms

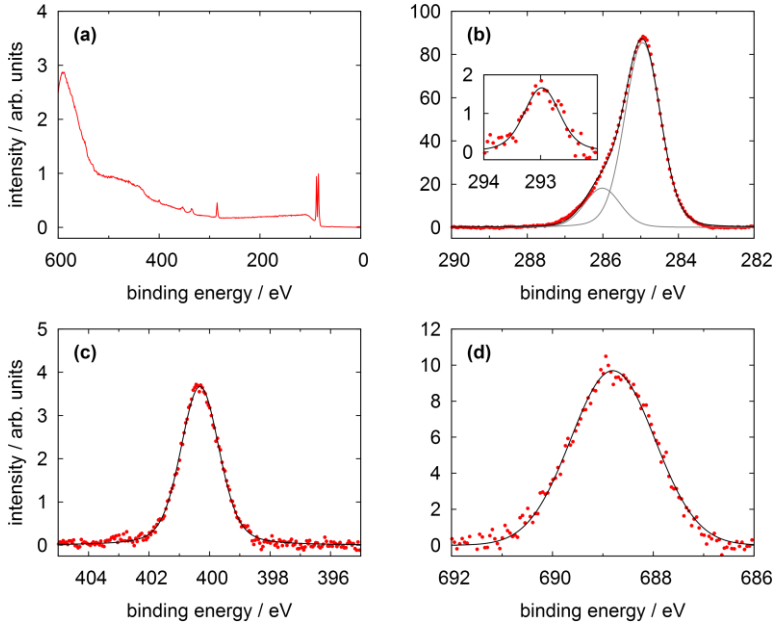

Figure S 7: XP spectra of a CF_3Azo-TATA multilayer on Au(111) showing (a) a survey spectrum, (b) the C 1s, (c) the N 1s and (d) the F 1s region.

Table S 8: Quantitative analysis of the XPS results of CF_3Azo-TATA multilayer. * Only the direct fitting errors are given. The total error cannot be inferred in a straight-forward manner and is estimated to be 15 %.

element	binding energy (eV)*	relative intensity*	calc. stoichiometry	assignment
C 1s	284.9 ± 0.1	0.812 ± 0.051	0.793	arom. + aliph.
	286.0 ± 0.1	0.173 ± 0.012	0.190	C-N
	293.0 ± 0.1	0.015 ± 0.001	0.017	C-F
N 1s	400.3 ± 0.1	0.035 ± 0.002	0.086	all N atoms
F 1s	688.8 ± 0.1	0.031 ± 0.006	0.052	all F atoms

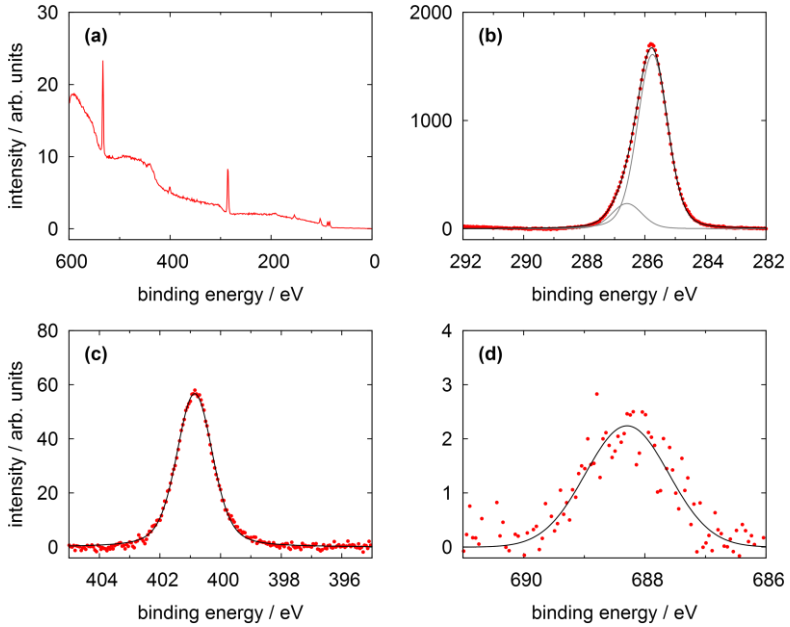

Figure S 9: XP spectra of a FAzo-TATA multilayer on Au(111) showing (a) a survey spectrum, (b) the C 1s, (c) the N 1s and (d) the F 1s region.

Table S 10: Quantitative analysis of the XPS results of FAzo-TATA multilayer. * Only the direct fitting errors are given. The total error cannot be inferred in a straight-forward manner and is estimated to be 15 %.

element	binding energy (eV)*	relative intensity*	calc. stoichiometry	assignment
C 1s	285.7 ± 0.1	0.873 ± 0.073	0.789	arom. + aliph.
	286.6 ± 0.1	0.127 ± 0.014	0.193	C-N
			0.018	C-F
N 1s	400.9 ± 0.1	0.031 ± 0.002	0.088	all N atoms
F 1s	688.3 ± 0.1	0.003 ± 0.001	0.018	all F atoms

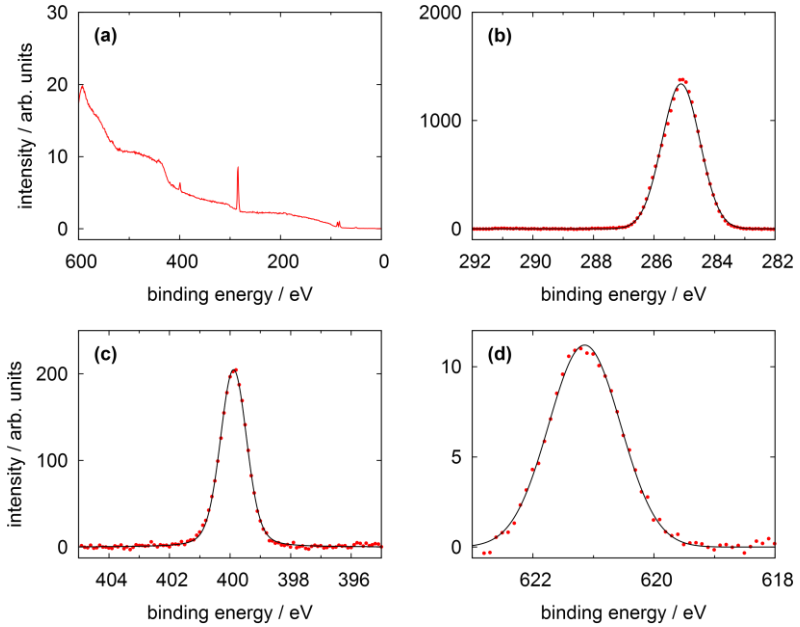

Figure S 11: XP spectra of a IAzo-TATA multilayer on Au(111) showing (a) a survey spectrum, (b) the C 1s, (c) the N 1s and (d) the I $3d_{5/2}$ region.

Table S 12: Quantitative analysis of the XPS results of IAzo-TATA multilayer. * Only the direct fitting errors are given. The total error cannot be inferred in a straight-forward manner and is estimated to be 15 %.

element	binding energy (eV)*	relative intensity*	calc. stoichiometry	assignment
C 1s	285.1 ± 0.1	1.000 ± 0.039	0.807	arom. + aliph.
N 1s	399.9 ± 0.1	0.153 ± 0.005	0.088	all N atoms
I 3d	621.1 ± 0.1	0.003 ± 0.001	0.018	all I atoms

2. Additional NEXAFS spectra

2.1 Monolayer

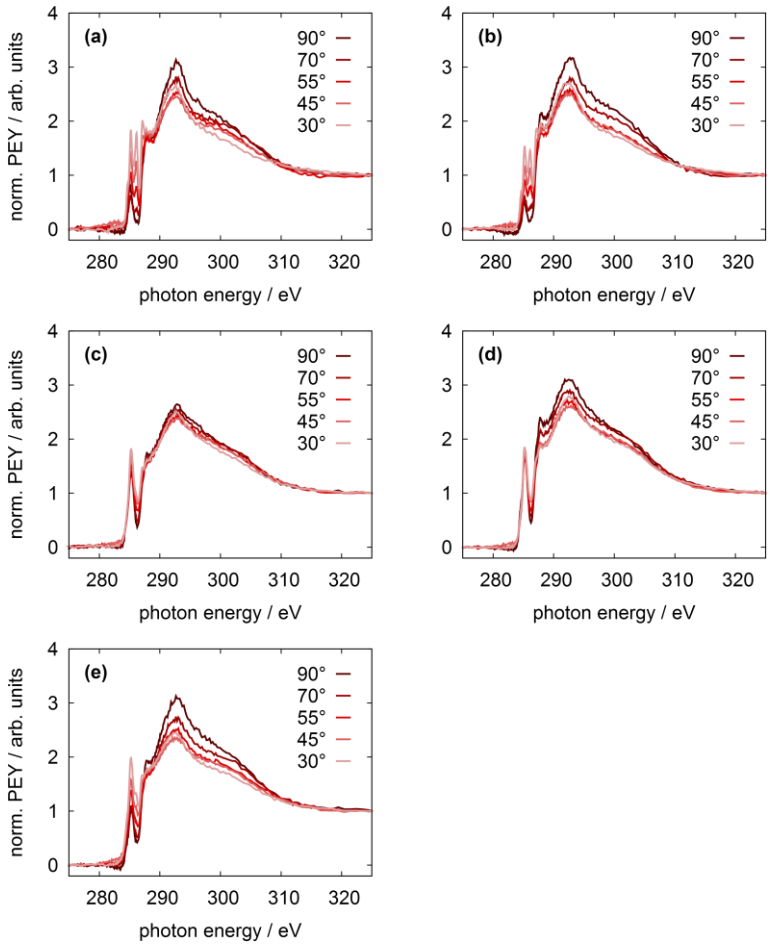

Figure S 13: NEXAFS spectra of C K-edge of (a) a TATA, (b) a Me-TATA, (c) a CF_3Azo-TATA, (d) a FAzo-TATA-, (e) a IAzo-TATA monolayer.

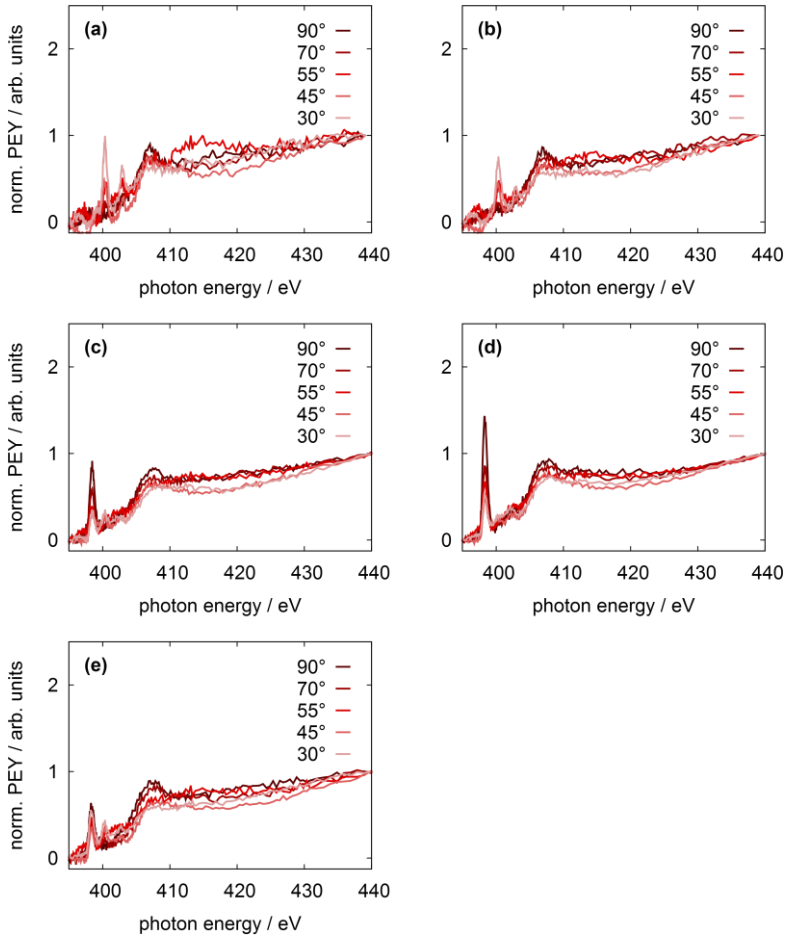

Figure S 14: NEXAFS spectra of N K-edge of (a) a TATA, (b) a Me-TATA, (c) a CF_3Azo-TATA, (d) a FAzo-TATA, (e) a IAzo-TATA monolayer.

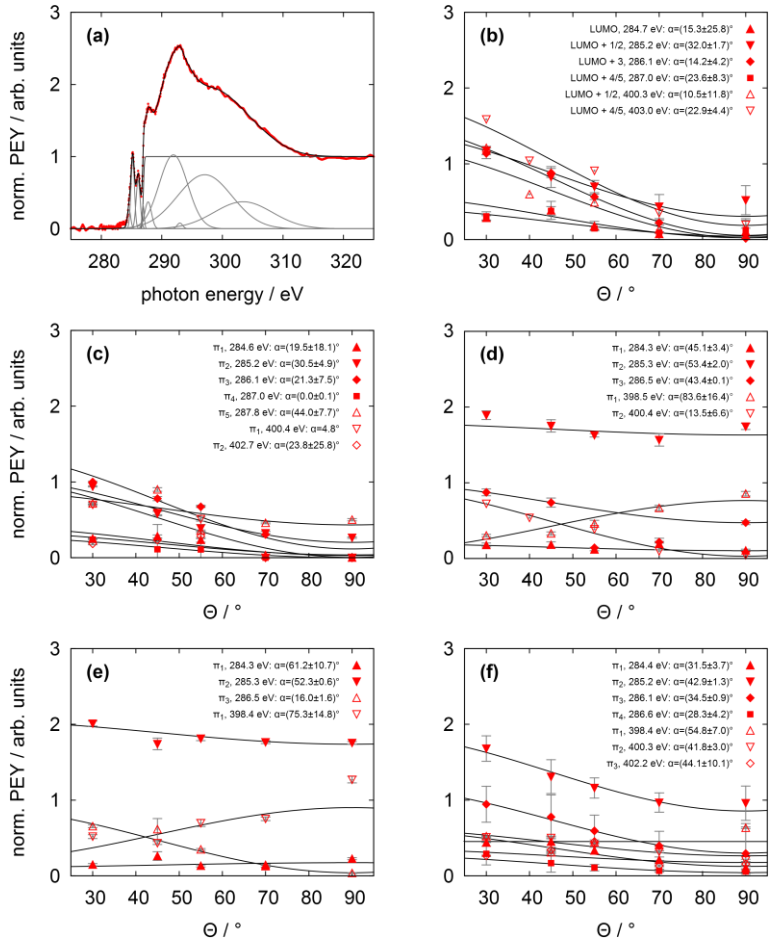

Figure S 15: Survey plots for determination of the angle dependency of the individual π* resonances of (a,b) a TATA, (c) a Me-TATA, (d) a CF_3Azo-TATA, (e) a FAzo-TATA, (f) a IAzo-TATA monolayer.

Table S 16: NEXAFS spectral analysis of Me-TATA monolayer on Au(111) single crystal. The resonances at the various energies are given in eV, the angles are defined with respect to the surface.

resonance	C 1s (Δ)	angle	N 1s (Δ)	angle
π_1	284.6 (0.0)	19.5 ± 18.1	400.4 (0.0)	4.8 ± 0.1
π_2	285.2 (0.6)	30.5 ± 4.9	402.7 (2.3)	23.8 ± 25.8
π_3	286.1 (1.5)	21.3 ± 7.5		
π_4	287.0 (2.4)	44.0 ± 7.7		
π_5	287.8 (3.2)	44.0 ± 7.7		

2.2 Multilayer

Comparing the individual monolayers with their thin multilayers, an additional π* resonance at ~ 287.6 eV is observed at the C K-edge for all multilayers. This could be a transition quenched in the monolayer due to the adsorption on the surface. As already mentioned, additional calculations show an overlap of the molecular orbitals with orbitals from gold atoms at the substrate surface. Hence, the additional resonance in the multilayer can be assigned to the TATA molecules without these adsorbate-substrate interactions.

Also at the N K-edge the resonances at 402.0 eV and 402.1 eV appears to be much more pronounced in the FAzoTATA and the IAzoTATA multilayers (see Figure S11) compared to the respective monolayer (Figure S8). This indicates that this resonance is quenched by the interaction of the platform nitrogens with the gold substrate. At first sight surprisingly the CF_3AzoTATA does not show this effect, but the XPS intensity indicates that here only slightly more than a monolayer has been adsorbed and thus only a small fraction of the molecules appears to be decoupled from the gold substrate in this case. For a thicker multilayer also a pronounced resonance at ~ 402 eV would be expected.

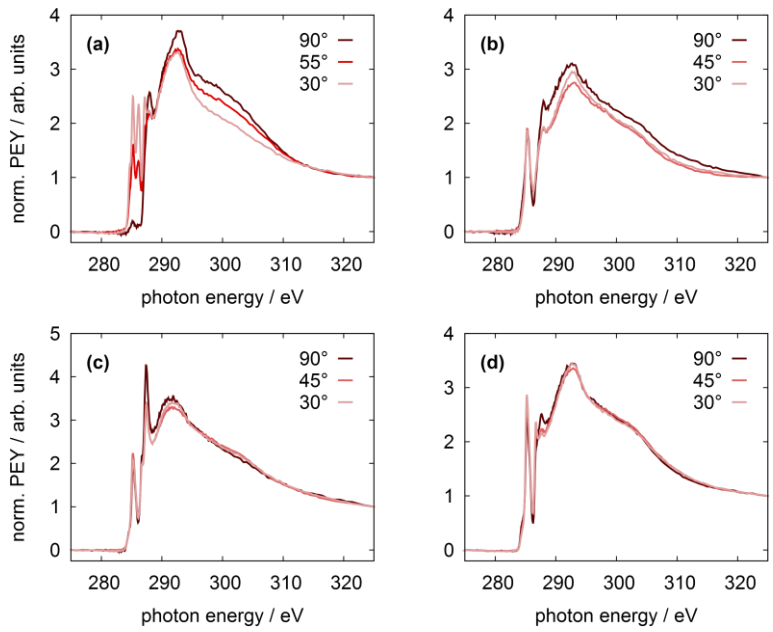

Figure S 17: NEXAFS spectra of C K-edge of (a) a TATA, (b) a CF_3Azo-TATA, (c) a FAzo-TATA, (d) a IAzo-TATA multilayer.

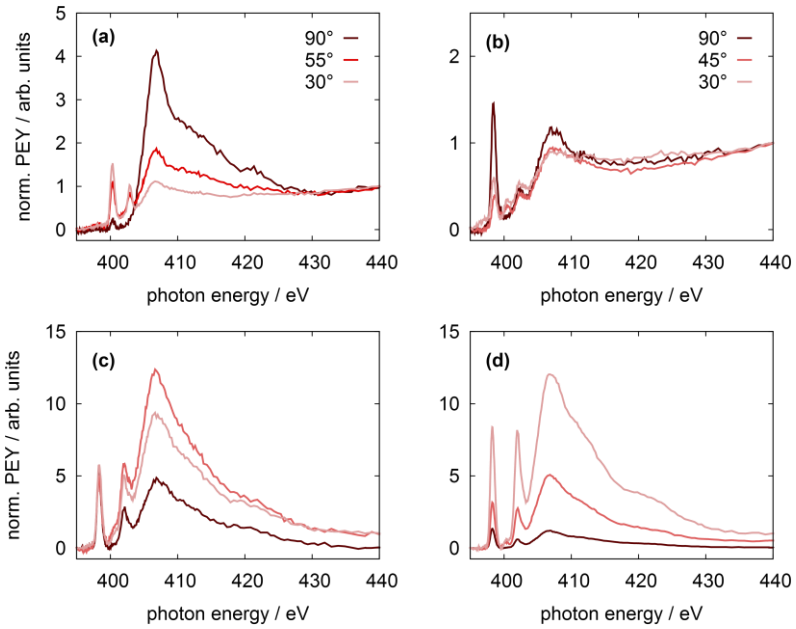

Figure S 18: NEXAFS spectra of N K-edge of (a) a TATA, (b) a CF_3Azo-TATA, (c) a FAzo-TATA, (d) a IAzo-TATA multilayer.

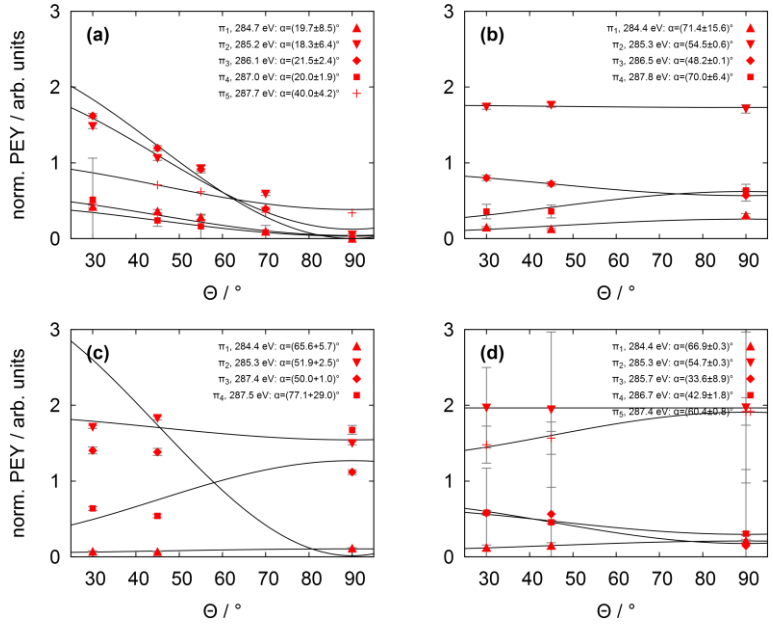

Figure S 19: Survey plots for determination of the angle dependency of the individual π* resonances of (a) a TATA, (b) a CF_3Azo-TATA, (c) a FAzo-TATA, (d) a IAzo-TATA multilayer.

Table S 20: NEXAFS spectral analysis of the thin Multilayers on Au(111) single crystal. The angles are defined with respect to the surface.

Molecule	resonance (eV)	angle (°)
TATA	284.7	19.7 ± 8.5
	285.2	18.3 ± 6.4
	286.1	21.5 ± 2.4
	287.0	20.0 ± 1.9
	287.7	40.0 ± 4.2
CF_3azo-TATA	284.4	71.4 ± 15.6
	285.3	54.6 ± 0.6
	286.5	48.2 ± 0.1
	287.8	70.0 ± 6.4
Fazo-TATA	284.4	65.6 ± 5.7
	285.3	51.9 ± 2.5
	287.4	50.0 ± 1.0
	287.5	77.1 ± 29.0
Iazo-TATA	284.4	66.9 ± 0.3
	285.3	54.7 ± 0.3
	285.7	33.6 ± 8.9
	286.7	42.9 ± 1.8
	287.4	60.4 ± 0.8

3. DFT Calculations

For the bare cation and the Me-TATA platform a range is given for the theoretical adlayer thickness because the arrangement of the alkyl chains is not exactly known. Based on published results alkyl chains of neighbouring molecules should align parallel to each other and to the surface in a so-called zigzag pattern, where all carbon atoms are in anti-conformation. This orientation reduces sterical hindrances and maximizes van der Waals interactions between each other and the surface. But this arrangement of the alkyl chains is not possible for the octyl-TATA platform because of the sterical hindrances, described in previous publications.[1] In addition, the distance between two TATA molecules on the surface is not large enough for complete planar adsorption of the alkyl chains. Thus, the alkyl chains may only partly lie on the surface and can also be found between the molecules above the surface. We therefore considered two models for the calculation of the layer thickness. The so-called gauche conformation, which gives the smallest layer thickness, and a general anti conformation, in which the side chains are standing upright from the surface (illustrated in Figure 13).

1 a) N. Hauptmann, K. Scheil, T. G. Gopakumar, F. L. Otte, C. Schütt, R. Herges, R. Berndt, *J. Am. Chem. Soc.* 2013, **24**, 8814-8817, http://dx.doi.org/10.1021/ja4036187; b) S. Lemke, S. Ulrich, F. Claußen, A. Bloedorn, U. Jung, R. Herges and O. M. Magnussen, *Surface Science*, 2015, **632**, 71–76, http://www.sciencedirect.com/science/article/pii/S0039602814002611.

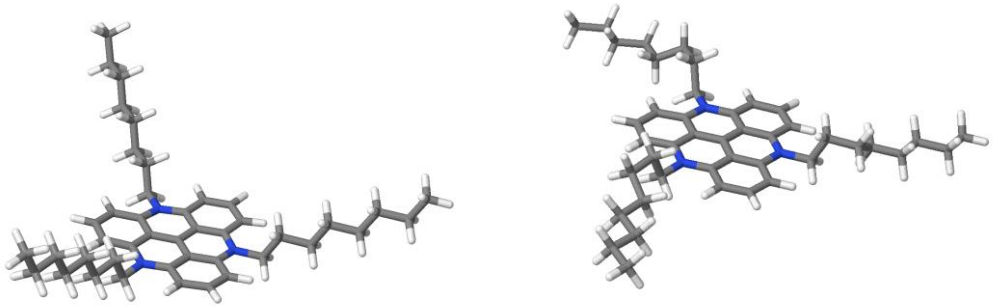

Figure S 21: Image of TATA cation (left: all anti and right in “gauche structure”).

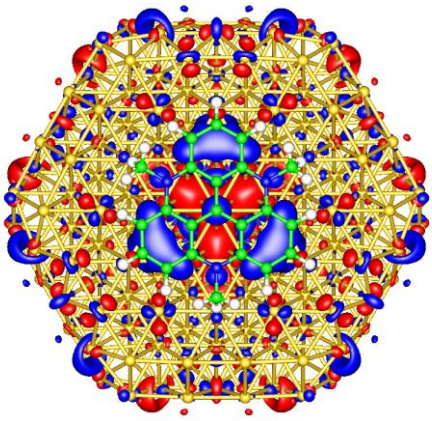

Figure S 22: Contour plot of HOMO-2 of the TATA cation on a gold cluster (PBE/SVP).

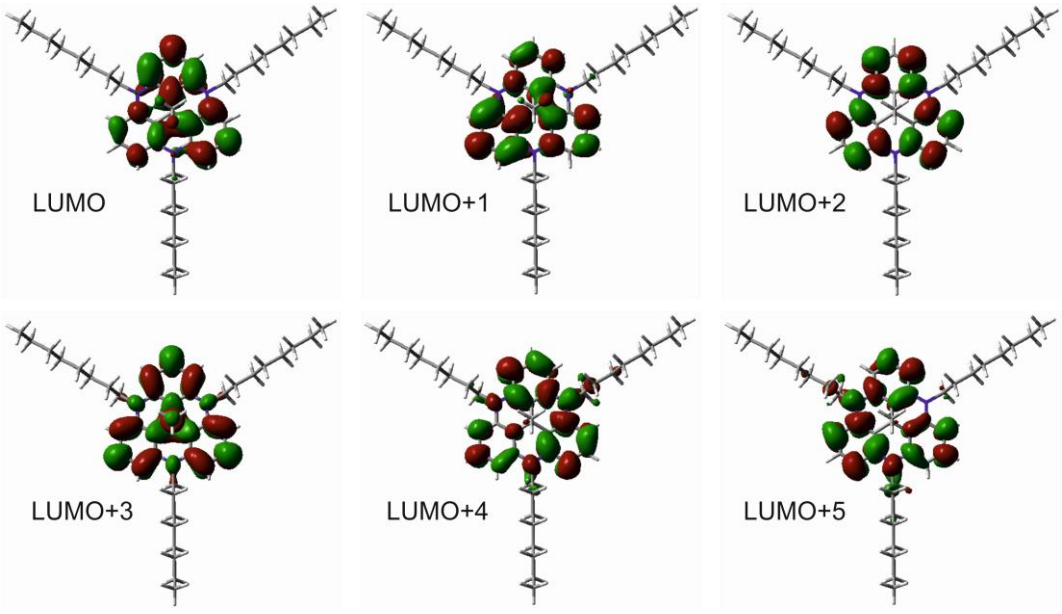

Figure S 23: Contour plots of LUMO to LUMO+5 of the free Me-TATA platform (B3LYP/6-31G*).

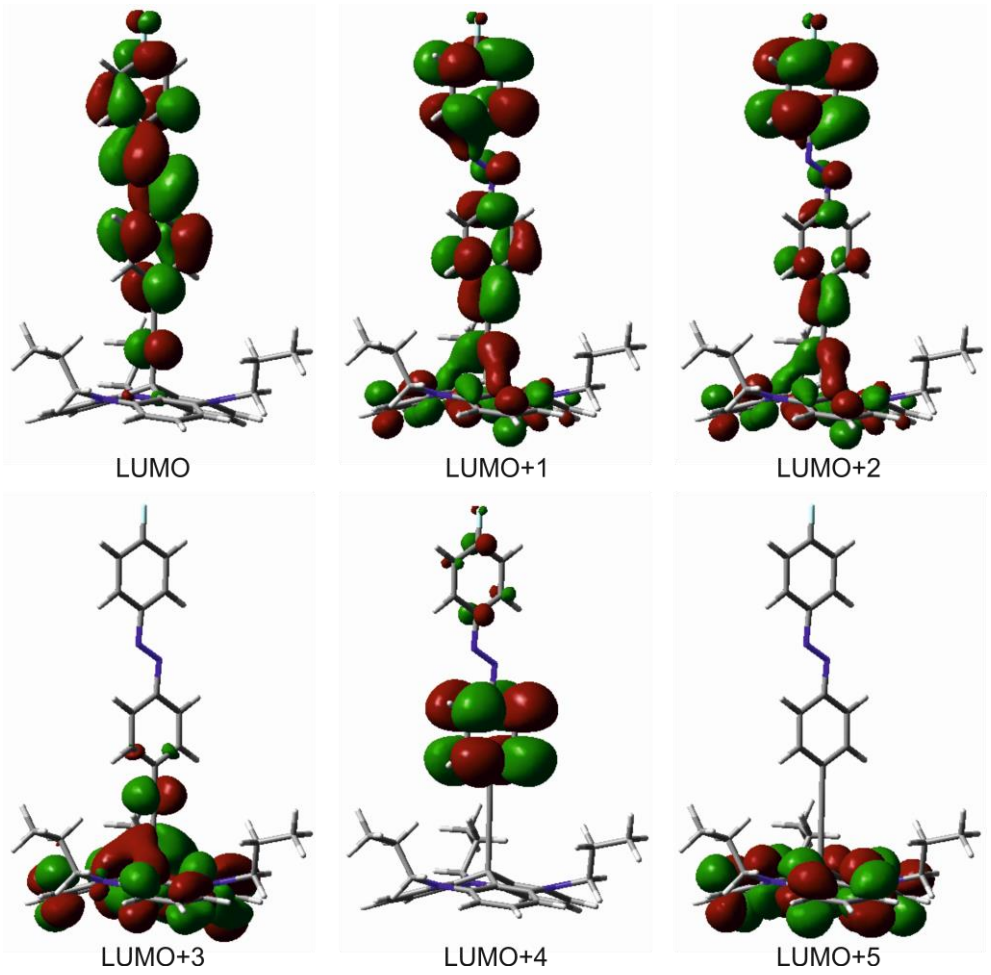

Figure S 24: Contour Plots of LUMO to LUMO+5 of the free Fazo-TATA platform.

Table S 25: Energy differences of the LUMO+x with respect to the LUMO of the individual platform molecules calculated at the B3LYP/6-31G* level of density functional theory.

molecular orbital	ΔE to LUMO (eV) **TATA**	ΔE to LUMO (eV) **Me-TATA**	ΔE to LUMO (eV) **CF_3azo-TATA**	ΔE to LUMO (eV) **Fazo-TATA**
LUMO	0.0000	0.0000	0.0000	0.00000
LUMO+1	1.3421	0.0000	1.9331	1.82835
LUMO+2	1.3421	0.1347	2.1084	1.96767
LUMO+3	1.7094	0.5306	2.3037	2.11761
LUMO+4	2.9682	1.2640	2.3269	2.19217
LUMO+5	2.9682	1.2640	2.5386	2.41530
LUMO+6	3.6793	1.9029	2.6322	2.47626
LUMO+7	4.1968	2.1788	2.7794	2.56061
LUMO+8	4.6075	2.1788	3.1824	3.21559
LUMO+9	4.6075	2.4610	3.4333	3.21859
LUMO+10	4.9114	2.5108	3.4616	3.35492

4. Synthesis

NMR spectra were recorded using a Bruker DRX 500 [^{1}H NMR (500 MHz), ^{13}C NMR (125.8 MHz)]. Mass spectra were obtained on a MALDI-MS-TOF Biflex III, Fa. Bruker-Daltonics. IR spectra were recorded with a Perkin-Elmer 1600 series FT-IR spectrometer, using a golden-gate diamond ATR unit A531-G. UV/Vis spectra were recorded with a Lambda 14 UV/Vis spectrometer, Fa. Perkin Elmer.

Synthesis of 12c-methyl-4,8,12-tri-*n*-octyl-4,8,12-triazatriangulene

Under nitrogen atmosphere and ice cooling 200 mg (284 µmol) 4,8,12-Tri-*n*-octyl-4,8,12-triazatriangulenium tetrafluoroborate was dissolved in 300 mL tetrahydrofuran and 50 µL (331 µmol) *N*,*N*,*N´*,*N´*-tetramethylethylenediamine and 9.00 mL (14.4 mmol) Methyllithium (1.6 M in diethyl ether) were added. After stirring for three hours while it was warming up to room temperature, the mixture was poured into 150 mL ice water. The mixture was extracted with diethyl ether and the combined organic layers were dried with magnesium sulfate. After evaporating the solvents the residue was filtered through a short column of florisil with a mixed solvent (diethyl ether / dichloromethane 10:1). The solvents were evaporated, yielding a colorless viscous oil (148 mg, 233 µmol, 82 %).

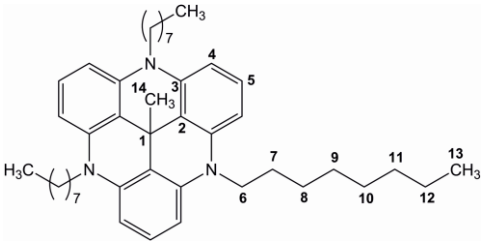

δ_H(500 MHz; $CDCl_3$) 7.17 (3 H, t, *J* = 8.2 Hz, 5-H), 6.53 (6 H, d, *J* = 8.2 Hz, 4-H), 3.88 (6 H, t, *J* = 8.1 Hz, 6-H), 1.85 (6 H, m, 7-H), 1.45 (12 H, m, 8-, 9-H), 1.34 (18 H, m, 10-, 11-, 12-H), 1.16 (3 H, s, 14-H), 0.93 (9 H, t, *J* = 6.9 Hz, 13-H) ppm.

δ_C(125.8 MHz; $CDCl_3$) 140.03 (3-C), 127.33 (5-C), 113.39 (2-C), 104.25 (4-C), 46.38 (6-C), 31.82 (8-C), 29.69 (1-C), 29.34 (9-C), 28.89 (10-C), 27.41 (14-C), 27.11 (11-C), 25.63 (7-C), 22.64 (12-C), 14.09 (13-C) ppm.

m/z (MALDI-TOF) 634 (M^+), 618 (M - CH_3).

$\tilde{\nu}$ (ATR) 3097w, 3025w, 2953m, 2921s, 2851m, 1615s, 1580s, 1484s, 1457s, 1391s, 1240m, 1168s, 776m, 722s cm^{-1}.

λ_{max} (Dichloromethane) 330, 295, 271 nm.